Available online at www.sciencedirect.com
ScienceDirect
Journal of Sound and Vibration 300 (2007) 139–159
JOURNAL OF SOUND AND VIBRATION
www.elsevier.com/locate/jsvi

Coupling effect of flexible geared rotor on quick-return mechanism undergoing three-dimensional vibration

Jer-Rong Chang*

Department of Aircraft Engineering, Air Force Institute of Technology, 1 Jyulun Road, Gang-Shan Township, Kaoshiung County, Taiwan 820, ROC

Received 20 January 2005; received in revised form 15 May 2006; accepted 24 July 2006
Available online 16 October 2006

Abstract

Regarding the quick-return mechanism, some researchers have neglected the rotor-mechanism coupling effect, and other researchers have combined the quick-return mechanism with the motor but only considered the rotational motion of the rotor by assuming the rotor to be rigid and neglected the gear mesh dynamics. In the study, the rotor-mechanism coupling effect is investigated to find that the dynamic behaviors of the coupled system are different from those uncoupled systems. The coupling effect is mainly due to the flexibility of the shaft, the bearing, and the gear mesh. When the quick-return mechanism is driven with the flexible geared rotor, the vibrations of the geared rotor have significant influences on the dynamic behaviors of the quick-return mechanism. The traditional studies formulated the quick-return mechanism only under the consideration of planar motion. However, the three-dimensional vibration has to be considered for establishing the physical model of the coupled system. The system model is formulated by using finite element method and following Hamiltonian approach. The numerical integration method is applied to obtain the dynamic response. The coupling effect of the geared rotor on the quick-return mechanism undergoing three-dimensional vibration is discussed by the parameter study. It is shown that the bearing stiffness and damping, the shaft radius and the gear transmission error excitation of the meshing gears have significant influences on the dynamic behavior of the mechanism.

1. Introduction

Determination of critical speeds and dynamic responses of rotor systems is of vital importance in the design of geared rotor-bearing systems. A considerable amount of work has been reported [1,2]. Transient response analysis is often necessary to avoid possible low cycle fatigue caused by suddenly applied loads acting for a short duration. The most important disturbances creating abnormal pulsating torques in a turbo-alternator shafting system are: short circuit at generator terminals, faulty synchronizing, short circuit clearing, and line switching [1]. Sudden short circuit at generator terminals considered as the most unfavorable condition, sets up large torques in the rotor and induces severe stresses of the order of 4–5 times the normal values [3]. An accurate model is needed to perform such transient response analysis.

*Tel.: +886 7 6254168; fax: +886 6 2017630.
E-mail address: jerrong.chang@msa.hinet.net.

0022-460X/$ - see front matter © 2006 Elsevier Ltd. All rights reserved.
doi:10.1016/j.jsv.2006.07.046

Nomenclature

A	area of cross-section
c	damping coefficient
c_{yy}, c_{zz}	direct damping coefficients of bearing
c_{yz}, c_{zy}	cross damping coefficients of bearing
d	diameter
E	Young's modulus
e	amplitude of transmission error excitation
$e_t(t)$	transmission error excitation
F	force
G	shear modulus
I	area moment of inertia
I_D	diametrical mass moment of inertia of the shaft
I_P	polar mass moment of inertia of the shaft
$\mathbf{i}$, $\mathbf{j}$, $\mathbf{k}$	unit coordinate vector
K'	shear form factor
k	stiffness
k_h, c_h	gear mesh stiffness and damping coefficient
k_{yy}, k_{zz}	direct stiffness coefficients of bearing
k_{yz}, k_{zy}	direct stiffness coefficients of bearing
L	length of the rod
l	length; length of element
$\mathbf{M}$	mass matrix
$\mathbf{N}$	nonlinear vector
N	mode shapes
$\mathbf{Q}$	generalized coordinates
$\boldsymbol{q}$	displacement vector of nodes
r	radius
s	distance measured along coordinate X
T	kinetic energy
t	time
U	potential energy
u	axial displacement in x direction
V, W	lateral displacements in (Y, Z) directions
W	work (with superscript)
v, w	lateral displacement in (y, z) directions
X, Y, Z	system fixed coordinates
$x_{r1}(t)$	position of the translating/rotating joint
α, B, Γ	rotation angles about (X, Y, Z) directions
β, γ	rotation angles about (y, z) directions
$\boldsymbol{\lambda}$	Lagrange multiplier
ρ	mass density
$\mathbf{\Phi}$	constraints
ϕ_p	pressure angle of gear pair
ϕ_0	crank angle
φ	$\angle OAB$
Ω	spin speed
Ω_t	tooth passing frequency
ω	angular speed

Subscripts

c	crank
G	mass center
h	gear mesh
$n+1$	translating/rotating joint
O	origin of the fixed frame
r	rod
y, z	Y, Z directions
1,2	driving and driven gear or shaft

Superscripts

b	bearing
c	crank
ct	constraint
d	disk
g	gear
r	rod
s	shaft

When the drive system incorporates gear transmission units, the lateral and torsional modes get coupled. Lund [4] considered such coupling in the torsional–lateral vibrations in a geared system of rotors. Kahraman et al. [5] developed a finite element model of a geared rotor system on flexible bearings, including rotary inertia, axial loading and stiffness and damping of the gear mesh. Shiau et al. [6] presented a hybrid method of the finite element method and the general polynomial expansion method to study the dynamic characteristics of geared rotor systems. Rao et al. [7] studied the effect of pressure angle on the natural frequencies and mode shapes of geared rotors. Choi and Mau [8] applied the transfer matrix method to analyze the free and forced vibration due to mass unbalance, gear mesh errors, and force coupling effects. Many authors (Gunter [9]; Childs and Graviss [10]) had shown the parameters, including the geometry of system, coefficients of bearings, inertia properties of rigid disk, and the distribution of the mass and stiffness of rotating assemblies, can significantly influence the dynamic characteristics of a rotor-bearing system.

The system with time-dependent domain is briefly reviewed as follows.

First, the systems with time-dependent domain are modeled by Galerkin's method. The quick-return mechanism was investigated by Beale and Scott [11,12] on the deflection and stability, whereas the rod was considered as a Euler–Bernoulli Beam. Spatial dependence was eliminated by using Galerkin's method with time-dependent pinned–pinned overhanging beam modes. Okuyiga and Ray [13] solved numerically the displacement of a slightly compressible liquid for the one-dimensional case. Lee [14] presented the dynamics of a flexible rod of a quick-return mechanism.

Second, systems with time-dependent domain are modeled by the FEM. Many works on the dynamics and stability of a flexible rod in a quick-return mechanism were based on the FEM. Song and Haug [15] and Yang and Sadler [16] employed the FEM in their works to investigate the dynamics of the flexible planar mechanisms. Fung and Lee [17] investigated the stability of a quick-return mechanism with time-dependent coefficients. The flexible multibody machine tool mechanism subjected to constant and chattering cutting forces was analyzed by Shabana and Thomas [18]. Fung and Chen [19] simulated the flexible rod of a quick-return mechanism driven by a PM synchronous servomotor by the FEM. A variable-domain beam finite element with the size being a prescribed function of time was formulated by Stylianou and Tabarrok [20]. For a translating and rotating beam, a transition finite element with variable stiffness introduced at the interface of the joint hub was addressed in Refs. [21,22].

The quick-return mechanism in this study connecting to the geared rotor is different from those in Scott and Beale [11,12], Lee [14] and Fung and Lee [17] where the geared rotor was not considered. Though the quick-return mechanism considered in Fung and Chen [19] included the reduction gear box and motor, the gear pair and the transmitting shafts are assumed to be rigid and only the rotational motion was taken into account. The dynamic behaviors of the quick-return mechanism in the traditional studies only modeled the system based on planar motion. The dynamics of three dimensional vibration is met in this coupled system. By combining the geared rotor dynamics, the dynamic behaviors of the quick-return mechanism can be obtained more accurately than those past studies. The rod of the quick-return mechanism and the shaft of the geared rotor are all flexible and modeled based on the Timoshenko beam theory. The finite element method is employed in the formulation of the physical model. The element length for shaft is time independent while for the rod of the quick-return mechanism is time dependent. Five degrees of freedom at each node of the shaft element are considered except the axial motion along the spinning direction and five degrees of freedom are also used for the rod node, which contain three translations and two lateral rotations. Then, Hamilton's principle is employed to derive the nonlinear governing equations with time-varying coefficients. The Runge–Kutta method is applied to obtain the dynamic response. The coupling effect of the geared rotor on the quick-return mechanism undergoing three-dimensional vibration has been investigated by the parameter studies. The studied parameters include the stiffness and the damping coefficient of the bearing, the mesh stiffness and pressure angle of the gear, and the shaft radius.

2. Formulations of physical model

The system embraces the geared rotor and the quick-return mechanism. The geared rotor including the bearing, the rigid disk, the gear set, and the flexible shaft transmits power to the quick-return mechanism. The crank of the quick-return mechanism studied in this paper is considered to be short. Compared with the long rod and the long shaft, the flexibility of the crank is neglected in this study. The undeformed and deformed configurations of the system are shown in Figs. 1 and 2, respectively.

2.1. Geared rotor

For geared rotor, the fixed frame O-XYZ is used, as shown in Fig. 2, and the unit vectors are denoted as $\{\mathbf{i}, \mathbf{j}, \mathbf{k}\}^{\mathrm{T}}$. Two translational displacements (V, W) the corresponding rotations (B, Γ) for lateral motion and the torsional displacement α are assumed to be small. The spin speed is denoted as Ω. The components of the

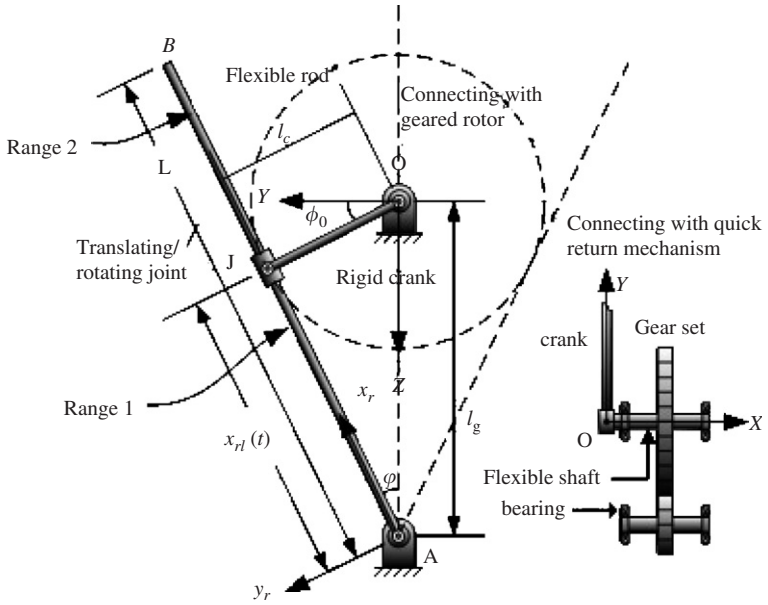

Fig. 1. Quick-return mechanism driven by geared rotor before deformation.

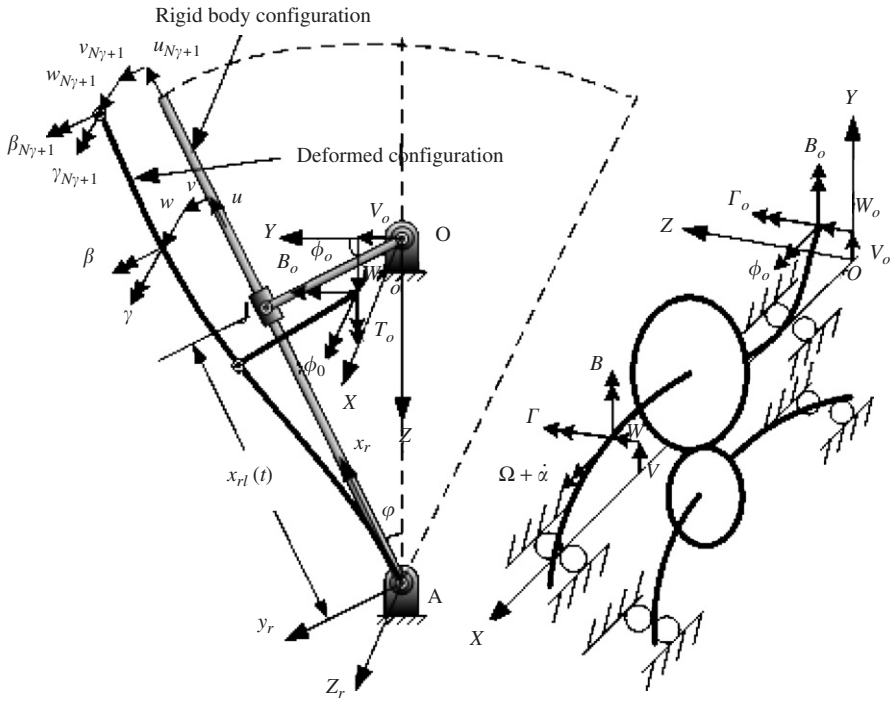

Fig. 2. Deformed rod and shafts of geared-rotor driven quick-return mechanism.

geared rotor are the rigid disk, the flexible shaft, the gear pair, and the bearing. The kinetic energy, the potential energy, and the virtual work of each component are derived to be applied in Hamiltonian approach.

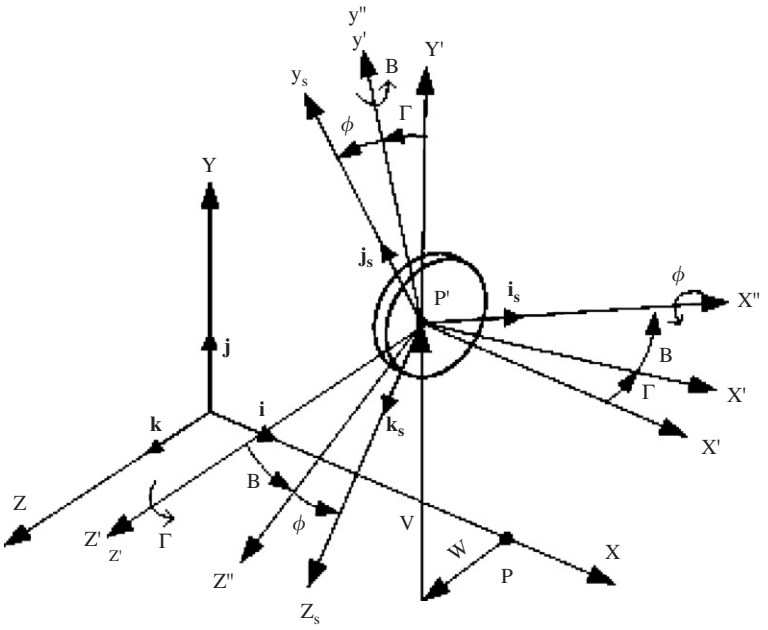

Fig. 3. A series of three rotations of reference frame: Γ about the $P'z'$-axis, B about the $P'y'$-axis, and ϕ about the $P'x'$-axis.

A disk in Y–Z plane is assumed to be rigid. To describe the rigid-body motion, a series of three rotations performed in the proper sequence as shown in Fig. 3, is sufficient to allow the frame to reach any orientation. The three rotations are:

1. A positive rotation Γ about the $P'Z'$-axis, resulting in the frame $P'-x'y'z'$.
2. A positive rotation B about the $P'y'$-axis, resulting in the frame $P'-x''y''z''$.
3. A positive rotation ϕ about the $P'x''$-axis, resulting in the frame $P'-x_sy_sz_s$.

The rotating reference frame $P'-x_sy_sz_s$ which attached to the cross-section of the shaft or the disk and their unit coordinate vectors are $\{\mathbf{i}_s, \mathbf{j}_s, \mathbf{k}_s\}^{\mathrm{T}}$. The rotational angle is given as $\phi = \Omega t + \alpha + \phi_s$, where ϕ_s is the initial angle. The spin speeds of the driving shaft and the driven shaft are denoted as Ω_1 and Ω_2, respectively, and they are related by $N_{t1}\Omega_1 = N_{t2}\Omega_2$ where N_{t1} and N_{t2} represent the tooth numbers of the driving and the driven gear.

2.1.1. Geared rotor: rigid disk

Using coordinate transformation, the relationship between the coordinate vectors $\{\mathbf{i}_s, \mathbf{j}_s, \mathbf{k}_s\}^{\mathrm{T}}$ and $\{\mathbf{i}, \mathbf{j}, \mathbf{k}\}^{\mathrm{T}}$ can be established. Since the lateral rotations are very small in practical, $\cos B \approx 1$, $\cos \Gamma \approx 1$, $\sin B \approx B$, and $\sin \Gamma \approx \Gamma$ are approximated. And neglecting the higher order terms of B and Γ, the following equations hold:

$$\begin{Bmatrix} \mathbf{i}_s \\ \mathbf{j}_s \\ \mathbf{k}_s \end{Bmatrix} = \begin{bmatrix} 1 & \Gamma & -B \\ B\sin\phi - \Gamma\cos\phi & \cos\phi & \sin\phi \\ \Gamma\sin\phi + B\cos\phi & -\sin\phi & \cos\phi \end{bmatrix} \begin{Bmatrix} \mathbf{i} \\ \mathbf{j} \\ \mathbf{k} \end{Bmatrix}. \tag{1}$$

The angular speed of the frame $P'-x_sy_sz_s$ is denoted as $\boldsymbol{\omega}_s = \omega_x\mathbf{i}_s + \omega_y\mathbf{j}_s + \omega_z\mathbf{k}_s$. It relates to the angular speed $\dot{\phi}\mathbf{i} + \dot{B}\mathbf{j} + \dot{\Gamma}\mathbf{k}$ as

$$\begin{Bmatrix} \omega_x \\ \omega_y \\ \omega_z \end{Bmatrix} = \begin{bmatrix} 1 & \Gamma & -B \\ B\sin\phi - \Gamma\cos\phi & \cos\phi & \sin\phi \\ \Gamma\sin\phi + B\cos\phi & -\sin\phi & \cos\phi \end{bmatrix} \begin{Bmatrix} \dot{\phi} \\ \dot{B} \\ \dot{\Gamma} \end{Bmatrix}. \tag{2}$$

Substituting Eq. (2) into Eq. (1) and neglecting the higher order terms of B and Γ, one can derive the kinetic energy of the disk for lateral and torsional motion as

$$\begin{aligned} T^d &= \frac{1}{2}\int_0^l \rho A(\dot{V}^2 + \dot{W}^2)\,\mathrm{d}s + \frac{1}{2}\int_0^l \rho\left\{I_P\omega_x^2 + I\left(\omega_y^2 + \omega_z^2\right)\right\}\mathrm{d}s \\ &= \frac{1}{2}\sum_{i=1}^{N_d}\left\{m_i^d\left[(\dot{V}_i^d)^2 + (\dot{W}_i^d)^2\right]\right\} + \frac{1}{2}\sum_{i=1}^{N_d}\left\{I_{Pi}^d\left(\Omega + \dot{\alpha}_i^d\right)^2 + I_{Di}^d\left[\left(\Gamma\dot{B}_i^d\right)^2 + \left(\dot{\Gamma}_i^d\right)^2\right]\right\} \\ &\quad + \frac{1}{2}\sum_{i=1}^{N_d}\left\{I_{Pi}^d\left(\Omega + \dot{\alpha}_i^d\right)\left(\Gamma_i^d\dot{B}_i^d - B_i^d\dot{\Gamma}_i^d\right)\right\}, \end{aligned} \tag{3}$$

where N_d is the number of the disk, and m_i^d, I_{Pi}^d, and I_{Di}^d express the mass, the polar and the diametrical moment of inertia of the ith disk, respectively.

2.1.2. Geared rotor: shaft element

Two-noded shaft element with 10 degrees of freedom is used in finite element analysis. The kinetic energy for the ith shaft element containing the torsional motion is

$$\begin{aligned} T_i^s &= \frac{1}{2}\int_0^l \rho\left\{A\left(\dot{V}^2 + \dot{W}^2\right) + I_D\left(\dot{B}^2 + \dot{\Gamma}^2\right) + I_p(\Omega + \dot{\alpha})^2\right\}\mathrm{d}s \\ &\quad + \frac{1}{2}\int_0^l \rho\left\{I_p(\Omega + \dot{\alpha})(\Gamma\dot{B} - B\dot{\Gamma})\right\}\mathrm{d}s, \end{aligned} \tag{4}$$

where l, ρ, A, I_p, and I_D are denoted as the length, the density, the area, the polar and the diametrical moment of inertia of the ith shaft element.

The total potential energy for the ith shaft element including bending deflection, shear deformation, and torsional deflection is given by

$$\begin{aligned} U_i^s &= \frac{1}{2}\int_0^l EI[(B')^2 + (\Gamma')^2]\,\mathrm{d}s + \frac{1}{2}\int_0^l GI_p(\alpha')^2\,\mathrm{d}s \\ &\quad + \frac{1}{2}\int_0^l K'GA[(V' - \Gamma)^2 + (W' + B)^2]\,\mathrm{d}s, \end{aligned} \tag{5}$$

where E, G, K' represent the Young's modulus, the shear modulus, and the shear form factor.

The deflections of an arbitrary cross-section within the shaft element are described in terms of the displacements of the two nodal points. The transformation relationship is

$$\begin{Bmatrix} V(s,t) \\ W(s,t) \\ B(s,t) \\ \Gamma(s,t) \\ \alpha(s,t) \end{Bmatrix} = \begin{bmatrix} N_{v1} & 0 & 0 & N_{v2} & 0 & N_{v3} & 0 & 0 & N_{v4} & 0 \\ 0 & N_{v1} & -N_{v2} & 0 & 0 & 0 & N_{v3} & -N_{v4} & 0 & 0 \\ 0 & -N_{\Gamma1} & N_{\Gamma2} & 0 & 0 & 0 & -N_{\Gamma3} & N_{\Gamma4} & 0 & 0 \\ N_{\Gamma1} & 0 & 0 & N_{\Gamma2} & 0 & N_{\Gamma3} & 0 & 0 & N_{\Gamma4} & 0 \\ 0 & 0 & 0 & 0 & N_{\alpha1} & 0 & 0 & 0 & 0 & N_{\alpha2} \end{bmatrix} \mathbf{q}^s(t)_i, \tag{6}$$

where

$$\mathbf{q}^s(t)_i = \begin{bmatrix} V_i & W_i & B_i & \Gamma_i & \alpha_i & V_{i+1} & W_{i+1} & B_{i+1} & \Gamma_{i+1} & \alpha_{i+1} \end{bmatrix}. \tag{7}$$

The vector $\mathbf{q}^s(t)_i$ represent the displacements of two nodes of the ith shaft element. And the mode shape functions N_{v1}, $N_{v2},\ldots,N_{\alpha2}$ are functions of the position s in local coordinate. The static-unit displacement functions are chosen as the mode shape functions based on the Timoshenko-beam theory. Giving a unit displacement at one node while fixing all the other displacements, one can derive the static displacements of

the element [6]. The mode shapes are given by

$$\begin{aligned} N_{v1} &= \frac{1}{1+\phi}\left[2a^3 - 3a^2 + 1 + \phi(1-a)\right] \qquad N_{v2} = \frac{l}{1+\phi}\left[a^3 - 2a^2 + a + \frac{\phi}{2}(-a^2 + a)\right] \\ N_{v3} &= \frac{1}{1+\phi}\left[-2a^3 + 3a^2 + \phi a\right] \qquad N_{v4} = \frac{l}{1+\phi}\left[a^3 - a^2 + \frac{\phi}{2}(a^2 - a)\right] \\ N_{\Gamma 1} &= \frac{1}{1+\phi}\left[\frac{1}{l}(6a^2 - 6a)\right] \qquad N_{\Gamma 2} = \frac{1}{1+\phi}\left[3a^2 - 4a + 1 + \phi(1-a)\right] \\ N_{\Gamma 3} &= \frac{1}{1+\phi}\left[\frac{1}{l}(-6a^2 + 6a)\right] \qquad N_{\Gamma 2} = \frac{1}{1+\phi}\left[3a^2 - 2a + \phi a\right] \\ N_{\alpha 1} &= 1 - a \qquad N_{\alpha 2} = a, \end{aligned} \tag{8}$$

where

$$\phi = \frac{12EI}{K'GAl^2}, \quad a = \frac{s}{l}. \tag{9}$$

2.1.3. Geared rotor: gear mesh

The gear mesh model only considers the planar responses. Fig. 4 shows a gear pair in which the teeth mesh is modeled with an equivalent stiffness k_h, a dashpot c_h and a displacement transmission error $e_t(t)$ along the pressure line. In the present model, the mesh stiffness and damping are considered to be constant. The transmission error is assumed to be sinusoidal with tooth passing frequency, i.e. $e_t(t) = e \sin \Omega_t t$. The gear mesh force along the pressure line is modeled by Rao et al. [7] as follows:

$$\mathbf{F}^g = -k_h \mathbf{S}_h \mathbf{q}^g - c_h \mathbf{S}_h \dot{\mathbf{q}}^g + \mathbf{R}_h, \tag{10}$$

where the forcing vector $\mathbf{F}^g$, the displacement vector $\mathbf{q}^g$, the coefficient matrix $\mathbf{S}_h$ and the forcing vector $\mathbf{R}_h$ are expressed as

$$\mathbf{F}^g = \begin{bmatrix} F^g_{Y1} & F^g_{Z1} & T^g_1 & F^g_{Y2} & F^g_{Z2} & T^g_2 \end{bmatrix}^{\mathrm{T}},$$

$$\mathbf{q}^g = \begin{bmatrix} V^g_1 & W^g_1 & \alpha^g_1 & V^g_2 & W^g_2 & \alpha^g_2 \end{bmatrix}^{\mathrm{T}},$$

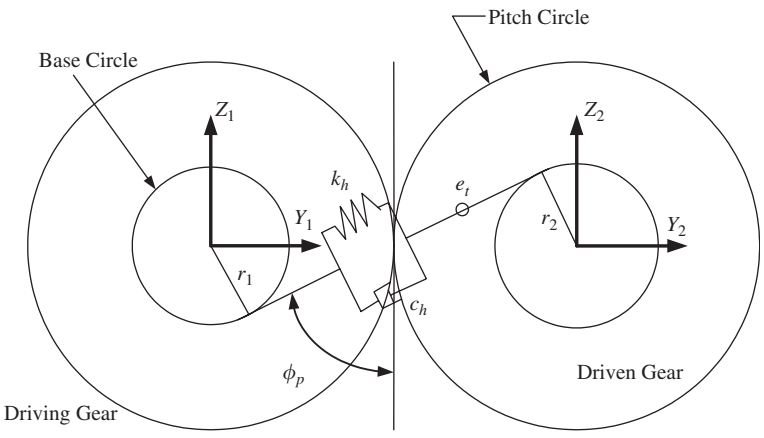

Fig. 4. Gear mesh model.

$$\mathbf{S}_h = \begin{bmatrix} s^2 & sc & r_1 s & -s^2 & -sc & r_2 s \\ sc & c^2 & r_1 c & -sc & -c^2 & r_2 c \\ r_1 s & r_1 c & r_1^2 & -r_1 s & -r_1 c & r_1 r_2 \\ -s^2 & -sc & -r_1 s & s^2 & sc & -r_2 s \\ -sc & -c^2 & -r_1 c & sc & c^2 & -r_2 c \\ r_2 s & r_2 c & r_1 r & -r_2 s & -r_2 c & r_2^2 \end{bmatrix},$$

$$\mathbf{R}_h = [\,-s \quad -c \quad -r_1 \quad s \quad c \quad -r_2\,]^{\mathrm{T}} e(k_h \sin \Omega_t t + c_h \Omega_t \cos \Omega_t t).$$

The symbols s and c used in the coefficient matrix $\mathbf{S}_h$ denote $\sin \phi_p$ and $\cos \phi_p$. The virtual work done by the gear mesh force is then given by

$$\delta W^g = \boldsymbol{\delta}\mathbf{q}^{g^{\mathrm{T}}} \mathbf{F}^g. \tag{11}$$

2.1.4. Geared rotor: bearing

The rotors supported by ball bearings considering the translation responses only have the corresponding force model which is expressed as

$$\mathbf{F}^b = -\begin{bmatrix} c_{yy} & c_{yz} \\ c_{zy} & c_{zz} \end{bmatrix} \begin{Bmatrix} \dot{V}^b \\ \dot{W}^b \end{Bmatrix} - \begin{bmatrix} k_{yy} & k_{yz} \\ k_{zy} & k_{zz} \end{bmatrix} \begin{Bmatrix} V^b \\ W^b \end{Bmatrix}. \tag{12}$$

The virtual work done by all the bearings is given as

$$\delta W^b = \sum_{j=1}^{N_b} \boldsymbol{\delta}\mathbf{q}_j^{b^{\mathrm{T}}} \mathbf{F}_j^b = -\sum_{j=1}^{N_b} \begin{Bmatrix} \delta V_j^b \\ \delta W_j^b \end{Bmatrix}^{\mathrm{T}} \times \left(\begin{bmatrix} c_{yy} & c_{yz} \\ c_{zy} & c_{zz} \end{bmatrix}_j \begin{Bmatrix} \dot{V}_j^b \\ \dot{W}_j^b \end{Bmatrix} + \begin{bmatrix} k_{yy} & k_{yz} \\ k_{zy} & k_{zz} \end{bmatrix}_j \begin{Bmatrix} V_j^b \\ W_j^b \end{Bmatrix} \right). \tag{13}$$

2.2. Quick-return mechanism

As shown in Figs. 1 and 2, the quick mechanism includes the rigid crank OJ with length l_c and the flexible rod AB with length L. The rod is driven by the crank by means of a translating/rotating joint. The symbol $x_{r1}(t)$ represents the current position of the translating/rotating joint. Other symbols in the figures are as follows: ϕ_0, crank angle, φ, angle between the z-axis and the undeformed axis of the flexible rod AB. Since the crank connecting to the shaft of the geared rotor at the origin O, the spatial motion instead of planar motion studied in the past have to be concerned due to the flexibility of the components of the geared rotor.

2.2.1. Quick-return mechanism: crank

The speed of mass center of the rigid crank v_G is expressed as

$$\mathbf{v}_G = \dot{V}_0 \mathbf{j} + \dot{W}_0 \mathbf{k} + \left(\dot{\phi}_0 \mathbf{i} + \dot{\mathrm{B}}_0 \mathbf{j} + \dot{I}_0 \mathbf{k}\right) \times \left(\frac{l_c}{2} \mathbf{j}_s\right). \tag{14}$$

The unit vector $\mathbf{j}_s$ can be arranged in terms of $\mathbf{i}$, $\mathbf{j}$, $\mathbf{k}$ by using Eq. (1). The kinetic energy for the rigid crank is derived as

$$T^c = \frac{1}{2} m_c v_G^2 + \frac{1}{2}\left(I_x \omega_x^2 + I_y \omega_y^2 + I_z \omega_z^2\right), \tag{15}$$

where m_c is the mass of the crank, and I_x, I_y, and I_z are the moment of inertia of mass center of the crank about x_s, y_s, and z_s axes, respectively. Substituting Eq. (14) into Eq. (15), one can know that the kinetic energy of the

crank is dependent on the five degrees of freedom, V_0, W_0, B_0, Γ_0, and ϕ_0 which are the vibration displacements at one end of the shaft connecting to the crank.

2.2.2. Quick-return mechanism: flexible rod

Since the translating/rotating joint moves reciprocally along the flexible rod AB, there is a time-dependent boundary involved. The total length L of the flexible rod is divided into two regions as shown in Fig. 1. The rod is divided into N_e elements for the finite element analysis. Regions 1 and 2 have m and n elements, respectively. Thus, total element number N_e equals $m+n$. In addition, $l_1(t)$ is the element length in region 1 for $x_{r1}(t) \leqslant x_r \leqslant L$ and $l_2(t)$ is the element length in region 2 for $0 \leqslant x_r \leqslant x_{r1}(t)$. The element lengths of the two regions are, respectively:

$$l(t) = \begin{cases} l_1(t) = \dfrac{L - x_{r1}(t)}{m}, & x_{r1}(t) \leqslant x_r \leqslant L, \\ l_2(t) = \dfrac{x_{r1}(t)}{n}, & 0 \leqslant x_r \leqslant x_{r1}(t) \end{cases} \tag{16}$$

and Eq. (16) satisfies the relationship

$$m l_1(t) + n l_2(t) = L. \tag{17}$$

To obtain the kinetic energy and the potential energy of the ith element of the deformed rod, the rotating frame $A{-}x_r y_r z_r$ attached to the AB rod is taken as the reference coordinates. The unit coordinate vectors and the angular velocity of the rotating frame are $\{\mathbf{i}_s, \mathbf{j}_s, \mathbf{k}_s\}^{\mathrm{T}}$ and $\dot{\varphi}\,\mathbf{k}_r$. The local coordinate of the ith element of the rod is chosen with $A'{-}xyz$. The rod is considered as Timoshenko beam and the beam element undergoing gross motion and elastic deformation is shown in Fig. 5.

The displacement field of the flexible rod modeled by the Timoshenko beam theory is

$$\begin{aligned} u_1(x, y, z, t) &= u(x, t) - y\gamma(x, t) + z\beta(x, t), \\ u_2(x, t) &= v(x, t), \qquad u_3(x, t) = w(x, t), \end{aligned} \tag{18}$$

where u and v represent the axial and transverse displacements of the flexible rod along the y and z directions, respectively, and β and γ are the slopes of the deflection curve along the y and z directions, respectively, due to bending deformation alone.

The deformed position vector of an arbitrary point P in the ith element is

$$\mathbf{r} = [r_i + x + u_1(x, y, z, t)]\mathbf{i}_r + u_2(x, t)\mathbf{j}_r + u_3(x, t)\mathbf{k}_r, \tag{19}$$

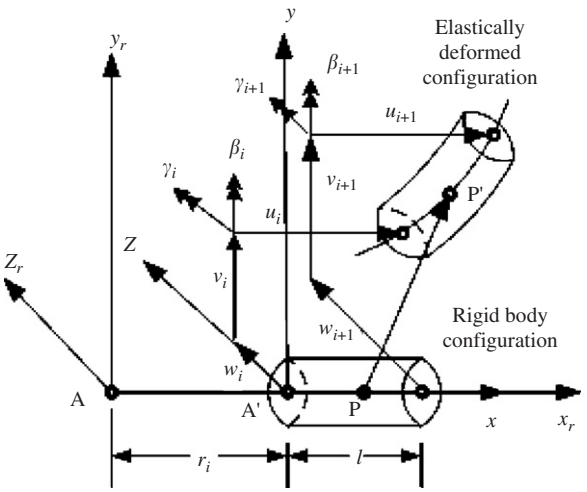

Fig. 5. The ith rod element undergoing gross motion and elastic deformation.

where vector $r_i\mathbf{i}_r$ locates the origin A' of the local coordinate system $A'-xyz$ of the ith beam element. Thus, the length r_i in regions 1 and 2 are, respectively,

$$r_i = \begin{cases} nl_2 + (i-1)l_1, & i = 1,\ldots,m, \\ (i-1)l_2, & i = 1,\ldots,n. \end{cases} \tag{20}$$

Then, by differentiating (20) with respect to time t, the absolute velocity vector is

$$\begin{aligned} \dot{\mathbf{r}} = {} & \left[\dot{r}_i + \dot{u} - y\dot{\gamma} + z\dot{\beta}\right]\mathbf{i}_r + \dot{v}\mathbf{j}_r + \dot{w}\mathbf{k}_r + \dot{\varphi}\mathbf{k}_r \\ & \times \left\{[r_i + x + u - y\gamma + z\beta]\mathbf{i}_r + v\mathbf{j}_r + w\mathbf{k}_r\right\}. \end{aligned} \tag{21}$$

The kinetic energy for the ith element is derived as

$$\begin{aligned} T_i^r &= \frac{1}{2}\int_{V_e} \rho\dot{\mathbf{r}}\cdot\dot{\mathbf{r}}\,\mathrm{d}V_e \\ &= \frac{1}{2}\int_0^l \rho A\left\{[\dot{r}_i + \dot{u} - v\dot{\varphi}]^2 + [\dot{v} + r_i\dot{\varphi} + u\dot{\varphi}]^2 + \dot{w}^2\right. \\ &\quad \left. + 2x\dot{\varphi}[\dot{v} + r_i\dot{\varphi} + u\dot{\varphi}] + x^2\dot{\varphi}^2\right\} + \rho I\left\{\left[\dot{\beta}^2 + \dot{\gamma}^2\right] + \left[\beta^2 + \gamma^2\right]\dot{\varphi}^2\right\}\mathrm{d}x, \end{aligned} \tag{22}$$

where $l(t)$ denotes the element length with $l_1(t)$ in region 1 and the element length $l_2(t)$ in region 2. ρ, A, and I are the density, the area of cross-section, and the diametrical area moment of inertia.

Using the Lagrange linear strains, the strain energy for the ith rod element due to bending, axial and shear deformations can be derived as

$$\begin{aligned} U_i^r = {} & \frac{1}{2}\int_0^l EI[(\beta')^2 + (\gamma')^2]\,\mathrm{d}x + \frac{1}{2}\int_0^l EA(u')^2\,\mathrm{d}x \\ & + \frac{1}{2}\int_0^l K'GA[(v'-\gamma)^2 + (w'+\beta)^2]\,\mathrm{d}x, \end{aligned} \tag{23}$$

where E, G, K' represent the Young's modulus, the shear modulus, and the shear form factor of the rod.

The deflections of an arbitrary cross-section within the rod element can be expressed in terms of the displacements of nodal points. The transformation relationship is established as

$$\begin{Bmatrix} u(x,t) \\ v(x,t) \\ w(x,t) \\ \beta(x,t) \\ \gamma(x,t) \end{Bmatrix} = \begin{bmatrix} N_{u1} & 0 & 0 & 0 & 0 & N_{u2} & 0 & 0 & 0 & 0 \\ 0 & N_{v1} & 0 & 0 & N_{v2} & 0 & N_{v3} & 0 & 0 & N_{v4} \\ 0 & 0 & N_{v1} & -N_{v2} & 0 & 0 & 0 & N_{v3} & -N_{v4} & 0 \\ 0 & 0 & -N_{\Gamma 1} & N_{\Gamma 2} & 0 & 0 & 0 & -N_{\Gamma 3} & N_{\Gamma 4} & 0 \\ 0 & N_{\Gamma 1} & 0 & 0 & N_{\Gamma 2} & 0 & N_{\Gamma 3} & 0 & 0 & N_{\Gamma 4} \end{bmatrix} \mathbf{q}^r(t)_i, \tag{24}$$

where

$$\mathbf{q}^r(t)_i = \begin{bmatrix} u_i & v_i & w_i & \beta_i & \gamma_i & u_{i+1} & v_{i+1} & w_{i+1} & \beta_{i+1} & \gamma_{i+1} \end{bmatrix}. \tag{25}$$

The vector $\mathbf{q}^r(t)_i$ represent the displacements of two nodes of the ith rod element. And the mode shape functions N_{u1}, N_{u2},…,$N_{\Gamma 1}$ are functions of the position x in local coordinate. The static-unit displacement functions are chosen as the mode shape functions based on the Timoshenko-beam theory. The mode shape functions can derived as

$$N_{u1} = 1 - a, \quad N_{u2} = a, \tag{26}$$

where $a = x/l$. The other mode shape functions are the same as those in Eq. (8).

2.3. Constraints

From the geometric relation of the triangle OAJ as shown in Fig. 1, the rigid-body motions x_{r1} and φ can be expressed in terms of ϕ_0 as

$$x_{r1} = \sqrt{l_g^2 + l_c^2 - 2l_c l_g \sin\phi_0}, \tag{27}$$

$$\varphi = \arcsin\left(\frac{l_c \cos\phi_0}{l_g}\right). \tag{28}$$

The associated velocity and acceleration can be obtained by differentiating the above equations with respect to time.

The unit coordinate vectors of the frame $A{-}x_r y_r z_r$ which attached to the rod can be related to the fixed frame O-XYZ by the following equation:

$$\begin{Bmatrix} \mathbf{i}_r \\ \mathbf{j}_r \\ \mathbf{k}_r \end{Bmatrix} = \begin{bmatrix} 0 & \sin\varphi & -\cos\varphi \\ 0 & \cos\varphi & \sin\varphi \\ 1 & 0 & 0 \end{bmatrix} \begin{Bmatrix} \mathbf{i} \\ \mathbf{j} \\ \mathbf{k} \end{Bmatrix}. \tag{29}$$

The translating/rotating joint is assumed to be a frictionless knife edge. The displacement and slope are continuous across the joint. The transverse displacements v_{n+1} and w_{n+1} and the rotational displacement β_{n+1} for the rod are constrained by the joint motion. Neglecting the higher order terms of V_0, W_0, B_0, and Γ_0, one has the following constraint equations for the deformed rod

$$\begin{aligned} &\tilde{u}_{n+1}\mathbf{i}_r + v_{n+1}\mathbf{j}_r + w_{n+1}\mathbf{k}_r \\ &\quad = l_c\left(B_0 \sin\phi_0 - \Gamma_0 \cos\phi_0\right)\mathbf{i} + V_0\mathbf{j} + W_0\mathbf{k}, \end{aligned} \tag{30}$$

where $\tilde{u}_{n+1}$ is the rigid-body motion in the $\mathbf{i}_r$ direction and is not constrained by the joint motion. Substituting Eq. (29) into Eq. (30), one can rearrange two constraint equations as follows:

$$\Phi^1 = v_{n+1} - V_0 \cos\varphi - W_0 \sin\varphi = 0, \tag{31}$$

$$\Phi^2 = w_{n+1} - l_c\left(\mathrm{B}_0 \sin\phi_0 - \Gamma_0 \cos\phi_0\right) = 0. \tag{32}$$

Under the assumption of small displacements B_0, and Γ_0, the constraint equation for β_{n+1} can be given as

$$\Phi^3 = \beta_{n+1} - B_0 \cos\varphi - \Gamma_0 \sin\varphi = 0. \tag{33}$$

In addition, the rod is hinged so that the displacements u_1, v_1, w_1, and β_1 are all zero.

The three constraints as expressed in Eqs. (31)–(33) are combined as the following form:

$$\mathbf{\Phi}(\mathbf{Q}) = \begin{bmatrix} \Phi^1 & \Phi^2 & \Phi^3 \end{bmatrix}^{\mathrm{T}} = \mathbf{0}. \tag{34}$$

The generalized coordinates $\mathbf{Q}$ is given by

$$\begin{aligned} \mathbf{Q} = [&V_1 \;\; W_1 \;\; \alpha_1 \;\; B_1 \;\; \Gamma_1 \;\; \cdots \;\; V_{N_s+1} \;\; W_{N_s+1} \;\; \alpha_{N_s+1} \;\; B_{N_s+1} \\ &\Gamma_{N_s+1} \;\; u_1 \;\; v_1 \;\; w_1 \;\; \beta_1 \;\; \gamma_1 \;\; \cdots \;\; u_1 \;\; v_1 \;\; w_1 \;\; \beta_1 \;\; \gamma_1 \cdots \\ &u_{N_r+1} \;\; v_{N_r+1} \;\; w_{N_r+1} \;\; \beta_{N_r+1} \;\; \gamma_{N_r+1}]^{\mathrm{T}}. \end{aligned} \tag{35}$$

Differentiating Eq. (34) with respect to time, one has the constraint velocity equation

$$\mathbf{\Phi}_{\mathbf{Q}}\dot{\mathbf{Q}} = \mathbf{0}. \tag{36}$$

Then differentiating Eq. (36) with respect to time, one has the constraint acceleration equation

$$\mathbf{\Phi}_{\mathbf{Q}}\ddot{\mathbf{Q}} = -\left(\mathbf{\Phi}_{\mathbf{Q}}\dot{\mathbf{Q}}\right)_{\mathbf{Q}}\dot{\mathbf{Q}} \equiv \boldsymbol{\eta}. \tag{37}$$

The generalized constraint reaction force can be obtained in terms of Lagrange multiplier $\boldsymbol{\lambda}$ as

$$\mathbf{F}^{ct} = \boldsymbol{\Phi}_{\mathbf{Q}}^{\mathrm{T}}\boldsymbol{\lambda}. \tag{38}$$

Hence, the virtual work done by all constraint reaction forces is

$$\delta W^{ct} = \delta\mathbf{Q}^{\mathrm{T}}\mathbf{F}^{ct}. \tag{39}$$

2.4. Hamilton's principle

Applying Hamilton's principle for the whole system, one has the variation equation

$$\int_{t_1}^{t_2}(\delta T^{d} + \sum_{i=1}^{Ns}\delta T_i^{s} + \delta T^{c} + \sum_{i=1}^{Nr}\delta T_i^{r} - \sum_{i=1}^{Ns}\delta U - \sum_{i=1}^{Nr}\delta U_i^{r} + \delta W^{g} + \delta W^{b} + \delta W^{ct})\,\mathrm{d}t = 0, \tag{40}$$

where δT^{d}, $\sum_{i=1}^{Ns}\delta T_i^{s}$, δT^{c}, and $\sum_{i=1}^{Nr}\delta T_i^{r}$ are the variations in the kinetic energy of the disk, the shaft, the crank, and the rod, respectively. $\sum_{i=1}^{Ns}\delta U_i^{s}$ and $\sum_{i=1}^{Nr}\delta U_i^{r}$ are the variations in the strain energy of the shaft and the rod. δW^{g}, δW^{b}, and δW^{c} are the virtual works done by the gear mesh force, the bearing forces, and the constraint forces, respectively. And the notations N_s and N_r represent the element numbers of the shaft and the rod, respectively.

Substituting Eqs. (3)–(5), (11), (13), (15), (22), (23), and (39) into Hamilton's principle (40), one can obtain the system equation of motion. The equation is expressed as

$$\mathbf{M}(\mathbf{Q})\ddot{\mathbf{Q}} + \mathbf{N}(\mathbf{Q},\dot{\mathbf{Q}}) + \boldsymbol{\Phi}_{\mathbf{Q}}^{\mathrm{T}}\boldsymbol{\lambda} = \mathbf{F}, \tag{41}$$

where $\mathbf{M}$, $\mathbf{N}$, and $\boldsymbol{\lambda}$ are mass matrix, nonlinear vector, and Lagrange multiplier, respectively. $\mathbf{F}$ is the forcing vector due to gear meshing transmission error. Since the translating/rotating joint is involved, the mass matrix is time dependent.

Combining the nonlinear ordinary differential Eq. (41) and the constraint acceleration Eq. (37), one obtains the following expression:

$$\begin{bmatrix} \mathbf{M} & \boldsymbol{\Phi}_{\mathbf{Q}}^{\mathrm{T}} \\ \boldsymbol{\Phi}_{\mathbf{Q}} & \mathbf{0} \end{bmatrix}\begin{bmatrix} \ddot{\mathbf{Q}} \\ \boldsymbol{\lambda} \end{bmatrix} = \begin{bmatrix} \mathbf{F} - \mathbf{N}(\mathbf{Q},\dot{\mathbf{Q}}) \\ \boldsymbol{\eta} \end{bmatrix}. \tag{42}$$

The above equation is the differential-algebraic equation (DAE) which governs the coupled system of the geared rotor and the quick-return mechanism.

2.5. Simplification of DAE

Using the partitioning method [23], the generalized coordinate vector is partitioned as

$$\mathbf{Q} = \begin{bmatrix} \mathbf{p}^{\mathrm{T}} & \mathbf{q}^{\mathrm{T}} \end{bmatrix}^{\mathrm{T}}, \tag{43}$$

where

$$\mathbf{p} = \begin{bmatrix} v_{n+1} & w_{n+1} & \beta_{n+1} \end{bmatrix}^{\mathrm{T}}, \tag{44}$$

$$\mathbf{q} = [V_1 \;\; W_1 \;\; \alpha_1 \;\; B_1 \;\; \Gamma_1 \;\; \cdots \;\; B_{N_s+1} \;\; \Gamma_{N_s+1} \;\; u_1 \;\; v_1 \;\; w_1 \;\; \beta_1 \times \gamma_1 \;\; \cdots \;\; u_{n+1} \;\; \gamma_{n+1} \;\; \cdots \;\; u_{N_r+1} \;\; v_{N_r+1} \;\; w_{N_r+1} \;\; \beta_{N_r+1} \;\; \gamma_{N_r+1}]^{\mathrm{T}}. \tag{45}$$

Then, Eq. (43) can be rewritten as

$$\begin{aligned}\mathbf{M}^{pp}\ddot{\mathbf{p}}+\mathbf{M}^{pq}\ddot{\mathbf{q}}+\mathbf{\Phi}_{\mathbf{p}}^{\mathrm{T}}\boldsymbol{\lambda}&=-\mathbf{N}^{p},\\ \mathbf{M}^{qp}\ddot{\mathbf{p}}+\mathbf{M}^{qq}\ddot{\mathbf{q}}+\mathbf{\Phi}_{\mathbf{q}}^{\mathrm{T}}\boldsymbol{\lambda}&=\mathbf{F}^{q}-\mathbf{N}^{q},\\ \mathbf{\Phi}_{\mathbf{p}}\ddot{\mathbf{p}}+\mathbf{\Phi}_{\mathbf{q}}\ddot{\mathbf{q}}&=\boldsymbol{\eta}.\end{aligned}\tag{46}$$

Eliminating $\boldsymbol{\lambda}$ and $\ddot{\mathbf{p}}$ from the above equation, one has the simplified second-order nonlinear ordinary differential equation in independent generalized coordinate $\mathbf{q}$ as

$$\hat{\mathbf{M}}(\mathbf{q})\ddot{\mathbf{q}}+\hat{\mathbf{N}}(\mathbf{q},\dot{\mathbf{q}})=0,\tag{47}$$

where

$$\begin{aligned}\hat{\mathbf{M}}&=\mathbf{M}^{qq}-\mathbf{M}^{qp}\mathbf{\Phi}_{\mathbf{p}}^{-1}\mathbf{\Phi}_{\mathbf{q}}-\mathbf{\Phi}_{\mathrm{q}}^{\mathrm{T}}\left(\mathbf{\Phi}_{\mathbf{p}}^{-1}\right)\quad\left[\mathbf{M}^{pq}-\mathbf{M}^{pp}\mathbf{\Phi}_{\mathbf{p}}^{-1}\mathbf{\Phi}_{\mathbf{q}}\right],\\ \hat{\mathbf{N}}&=\left[\mathbf{N}^{q}-\mathbf{F}^{q}-\mathbf{\Phi}_{\mathbf{q}}^{\mathrm{T}}\left(\mathbf{\Phi}_{\mathbf{p}}^{-1}\right)^{\mathrm{T}}\mathbf{N}^{p}\right]+\left[\mathbf{M}^{qp}\mathbf{\Phi}_{\mathbf{p}}^{-1}-\mathbf{\Phi}_{\mathbf{q}}^{\mathrm{T}}\left(\mathbf{\Phi}_{\mathbf{p}}^{-1}\right)^{\mathrm{T}}\mathbf{M}^{pp}\mathbf{\Phi}_{\mathbf{p}}^{-1}\right]\boldsymbol{\eta}.\end{aligned}\tag{48}$$

Let $\mathbf{X}=\begin{bmatrix}\mathbf{q}^{\mathrm{T}} & \dot{\mathbf{q}}^{\mathrm{T}}\end{bmatrix}^{\mathrm{T}}$ be the state variable vector, one can rewrite (47) in terms of $\boldsymbol{X}$ as

$$\dot{\mathbf{X}}=\begin{bmatrix}\dot{\mathbf{q}}\\ -\hat{\mathbf{M}}^{-1}\hat{\mathbf{N}}\end{bmatrix}.\tag{49}$$

Applying the Runge–Kutta integration method to solve Eq. (49), one can obtain the dynamic response of the coupled system.

3. Numerical results and discussions

The geared rotor-bearing system shown in Fig. 6 consists of two shafts and four bearings located at stations 1, 5, 6, and 10. The crank of the quick-return mechanism connects the shaft at station 11. The shaft is divided to four elements, and in each element the cross-sectional area is uniform with radius by 18.5 mm. The bearings are assumed isotropic and the bearing stiffness and damping coefficients are given as

$$\begin{aligned}k_{yy}=k_{zz}=k_b=10^6\,\mathrm{N/m},\quad k_{yz}=k_{zy}=0,\\ c_{yy}=c_{zz}=c_b=3000\,\mathrm{N\,s/m},\quad c_{yz}=c_{zy}=0.\end{aligned}$$

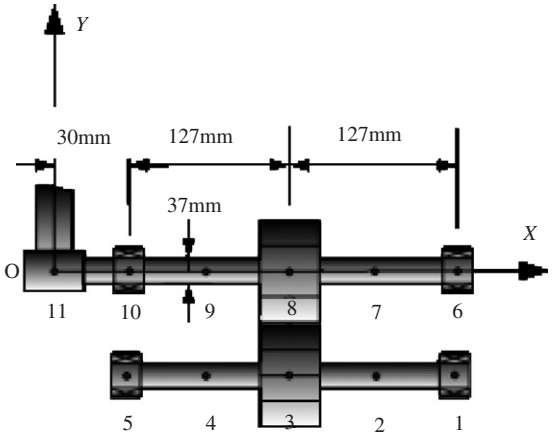

Fig. 6. Nodes of geared rotor-bearing system.

Table 1
Configuration data of geared rotor

Station no.	Axial distance to station 1 (mm)
1	0.0
2	63.5
3	127.0
4	190.5
5	254.0
6	0.0
7	63.5
8	127.0
9	190.5
10	254.0
11	284.0

Table 2
Gear pair data

Station no.	Mass (kg)	Polar inertia (kg/m^2)	Diametrical inertia (kg/m^2)
3	1.84	0.0018	0.0009
8	1.84	0.0018	0.0009

Tooth number = 28
Basic circle radii = 44.5 mm
$K_h = 10^8$ N/m, $c_h = 191.8$ N s/m, $\phi_p = 0^\circ$

The Young's modulus, the shear modulus and the density are $E = 20.7\,\mathrm{GN/m^2}$, $\rho = 7800\,\mathrm{kg/m^3}$ and $G = 79.5\,\mathrm{GN/m^2}$. Moreover, the gear pair with unit gear ratio is located at stations 3 and 8. The rotating speed is 100 rad/s. The other details of the geared rotor configuration are listed in Tables 1 and 2.

The parameters of the flexible rod have the same material properties and dimensions as in Refs. [11,19]. The parameters of the flexible quick-return mechanism involve the following dimensions and properties:

$$L = 1\,\mathrm{m},\ \ l_g = 0.59997\,\mathrm{m},\ \ l_c = 0.01 l_g,\ \ K' = 0.886,$$
$$G = 80\,\mathrm{GN/m^2},\ \ E = 70\,\mathrm{GN/m^2},\ \ I = 0.5208 \times 10^{-6}\,\mathrm{m^4},$$
$$\rho A = 7.15\,\mathrm{kg/m},\ \ d = 0.05\,\mathrm{m},\ \ m_c = 0.0429\,\mathrm{kg}.$$

Using the Runge–Kutta fourth-order numerical integration method, Eq. (49) is solved for the coupled system of the geared rotor and the quick-return mechanism. The deflections of the rod tip at point B in Fig. 1 under various conditions are plotted in the following figures to discuss the dynamic behaviors of the coupled system of the geared rotor and the quick-return mechanism.

First, following the similar way in the example studied by Fung and Chen [19], all the deflections at origin O are confined to be zeros except the constant crank angular speed input. The transverse deflection v of this uncoupled case is shown in Fig. 7 with 2-, 4-, 6-, and 8-element rod. It can be seen that the approximations are very close. The results of 4-, 6-, and 8-element rod approximations are indistinguishable. And the results coincide with those by Fung and Chen [19]. The tip deflection v at point B for the coupled system of the geared rotor and the quick-return mechanism is shown in Fig. 8 with 2-, 4-, 6-, and 8-element rod. It is shown that all the curves by using 2-, 4-, 6- and 8-element rod approximations are also almost coincident. The subsequent numerical results are obtained by using 6-element rod approximation.

The tip deflections at point B for coupled and uncoupled systems are plotted simultaneously in Fig. 9 to distinguish the differences between them. For the coupled system, the amplitude of the transverse deflection v is obviously larger than the transverse deflection w and the axial deflection u. However, the amplitude of the

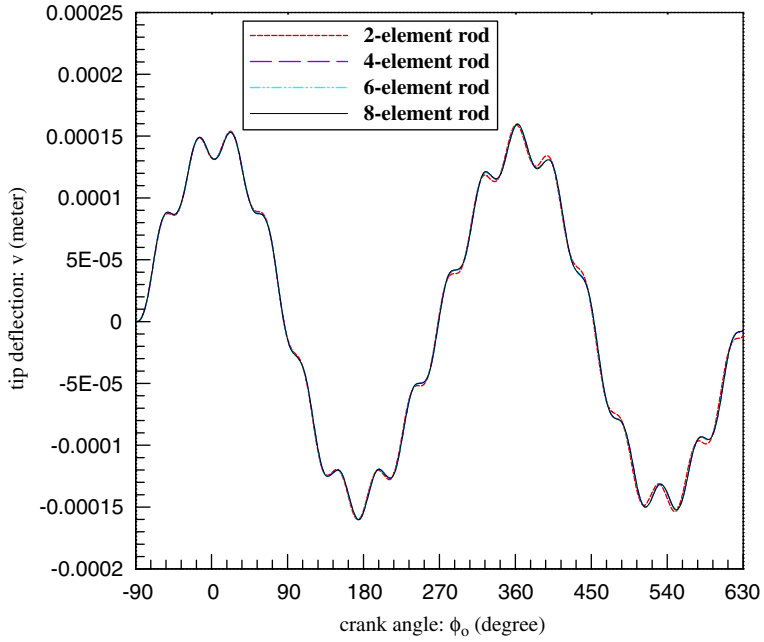

Fig. 7. The tip deflection v for uncoupled system.

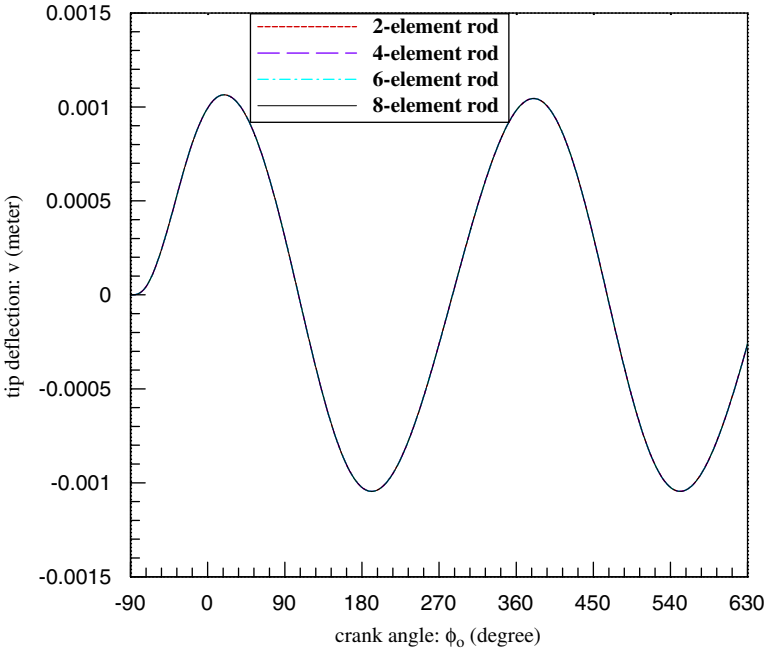

Fig. 8. The tip deflection v for coupled system.

transverse deflection w is about tenfold of the axial deflection u. This means w and u are of similar significance to a certain extent. The slope γ is far larger than the slope β. The deflections, v and γ, locate on the rotating plane so they are of larger amplitudes than w and β. For the uncoupled system, only the deflections, u, v, and γ are concerned so the deflections w and β. However, the differences between the deflections for the coupled and

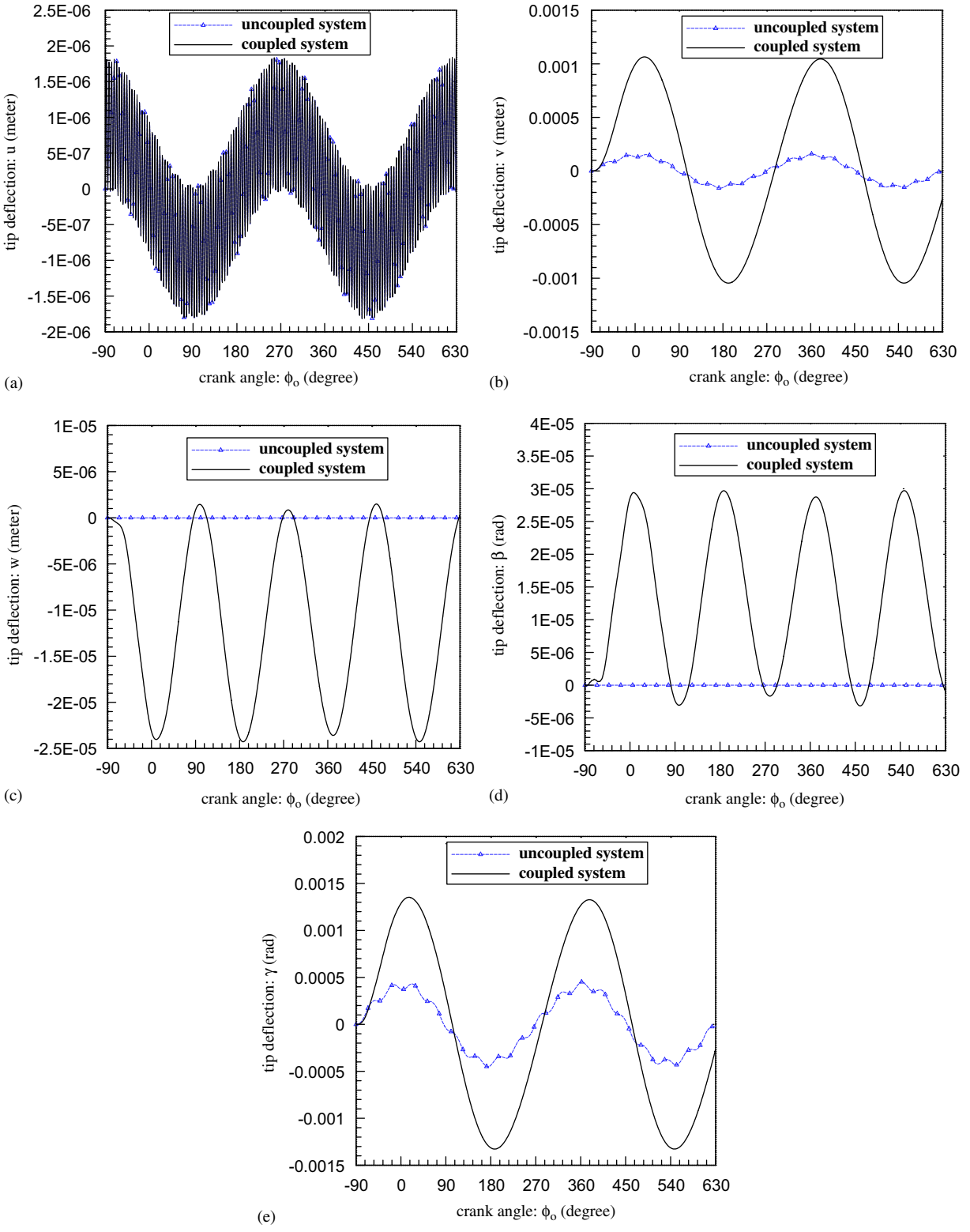

Fig. 9. The tip deflections for coupled and uncoupled systems.

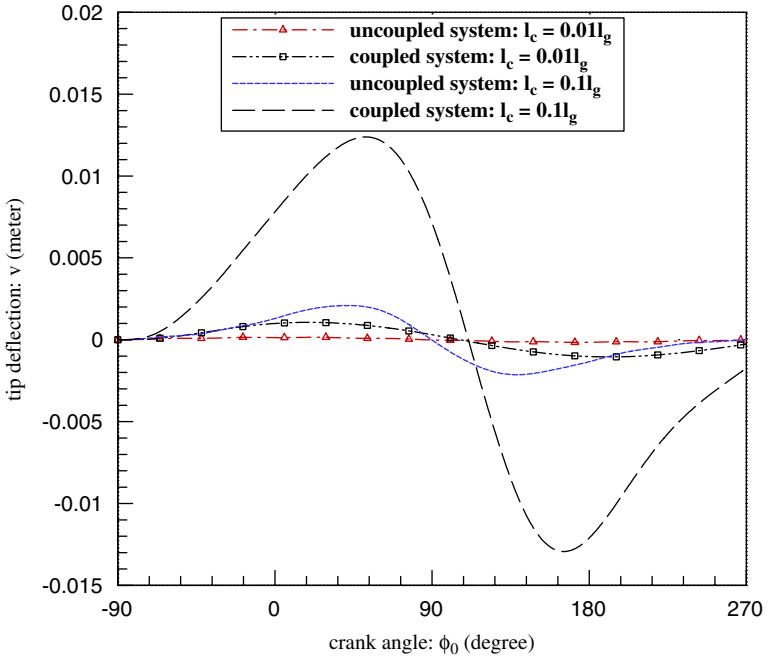

Fig. 10. The tip deflection v for coupled and uncoupled systems with different crank length: $l_c = 0.01l_g$, $0.1l_g$.

uncoupled systems are apparent to some extent. The axial deflection for both the two systems is almost the same. The deflections, v and γ, for the coupled system are larger than those for the uncoupled system. This means the influences of the flexibility of the geared rotor system on the quick-return mechanism are substantial.

Since crank length plays an important role on power transmission to the flexible rod in the quick-return mechanism, two different lengths of short crank for the coupled and uncoupled systems are studied. Fig. 10 only shows the tip deflection v. The deflection v for the coupled system is larger than that for the uncoupled system. Moreover, the longer crank induces larger tip deflection v for both systems.

For the coupled system, the parameters of the geared rotor may affect the dynamic behaviors of the quick-return mechanism. The parameters including the bearing stiffness, the bearing damping coefficient, the gear mesh stiffness, the gear pressure angle, and the shaft radius are investigated. The parameters as mentioned above are used except as described in the figures. And only the transverse deflection v is plotted.

First, the significance of the bearing stiffness is investigated. The bearing stiffness ranging from 10^6–10^9 N/m ($k_b = 10^6$, 10^7, 10^8, 10^9 N/m) are studied. The results are shown in Fig. 11. It is seen that the bearing stiffness has a significant influence on the tip deflection v for the coupled system. For the studied case, the stiffer bearing may suppresses the amplitude of the tip deflection v. The deflections for the coupled system with $k_b = 10^8$, 10^9 N/m almost near that for the uncoupled system. The effect of the bearing damping on the tip deflection is also studied. Four different values of the bearing damping coefficients ($c_b = 0$, 1500, 3000, 4500 N s/m) are compared as shown in Fig. 12. It is obvious that the rod tip oscillates when the undamped bearing is used. So proper damping of bearing may suppress the oscillation phenomenon.

To study the influence of the gear mesh on the quick-return mechanism, four different mesh stiffness values are used. They are 10^6, 10^7, 10^8, and 10^9 N/m. The results are shown in Fig. 13. It seems that the gear mesh stiffness has no influences on the coupling behavior. In addition, to study the influence of the pressure angle, three different values of the pressure angle are investigated. Fig. 14 shows that the pressure angle also has no influences on the coupling effect for the studied case. This implies that the uncoupled modes may be met since the spin speed is very low [7]. The influences of the gear transmission error excitation of the meshing gears are also investigated. The amplitude of transmission error between 0 and 9×10^{-4} m is studied. It is found that

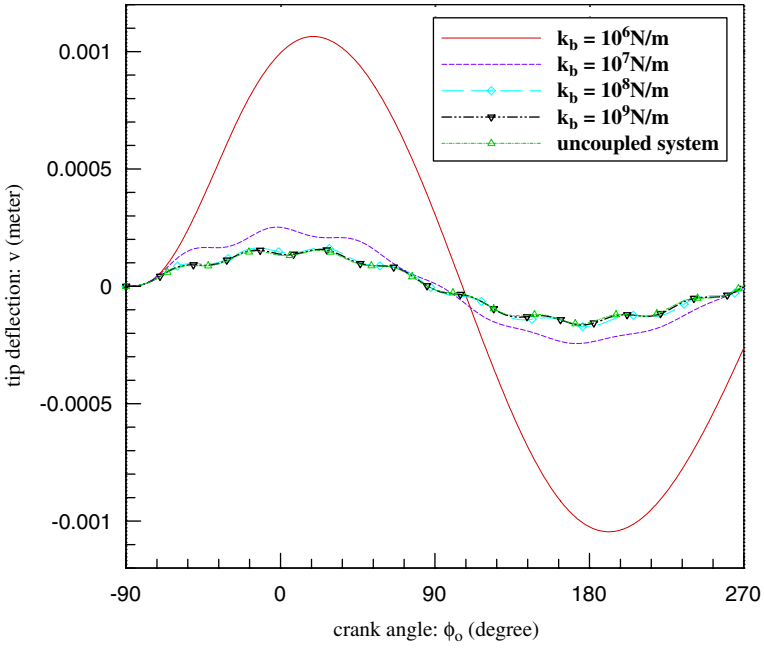

Fig. 11. The tip deflection v for coupled system with different bearing stiffness: $k_b = 10^6$, 10^7, 10^8, 10^9 N/m.

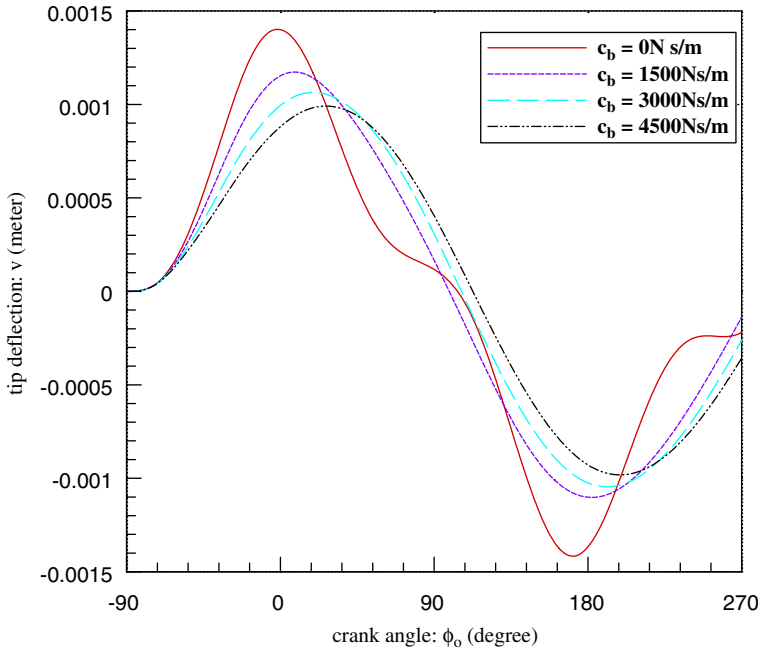

Fig. 12. The tip deflection v for coupled system with different bearing damping: $c_b = 0$, 1500, 3000, 4500 N s/m.

there is almost no influences when the bearing stiffness is $k_b = 10^6$ N/m. If $k_b = 10^7$ N/m is used, the influences of transmission error on the dynamic response are shown in Fig. 15. It is found that the transmission error induces high frequency oscillations and the severe oscillations occur when the transmission error is with larger amplitude. The oscillation is seen to be at tooth passing frequency (gear mesh frequency).

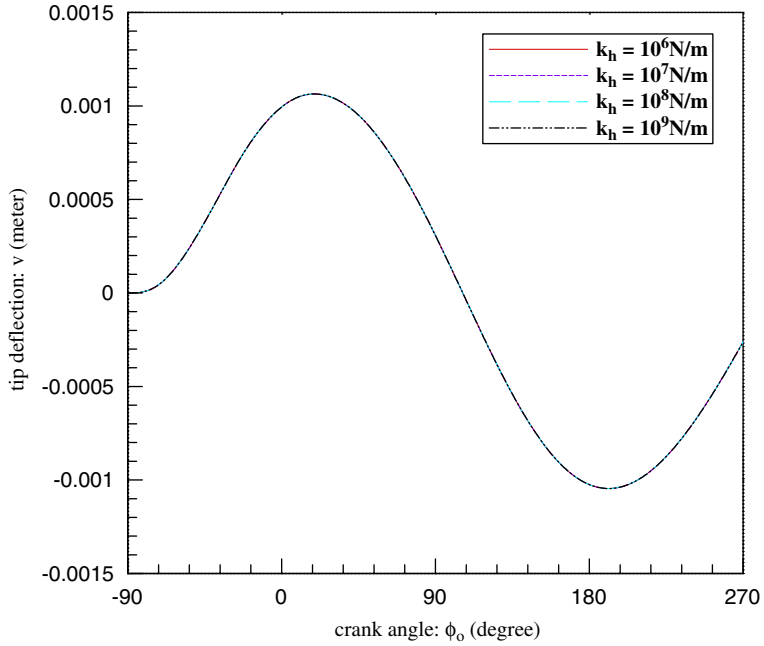

Fig. 13. The tip deflection v for coupled system with different gear mesh stiffness: $k_h = 10^6$, 10^7, 10^8, 10^9 N/m.

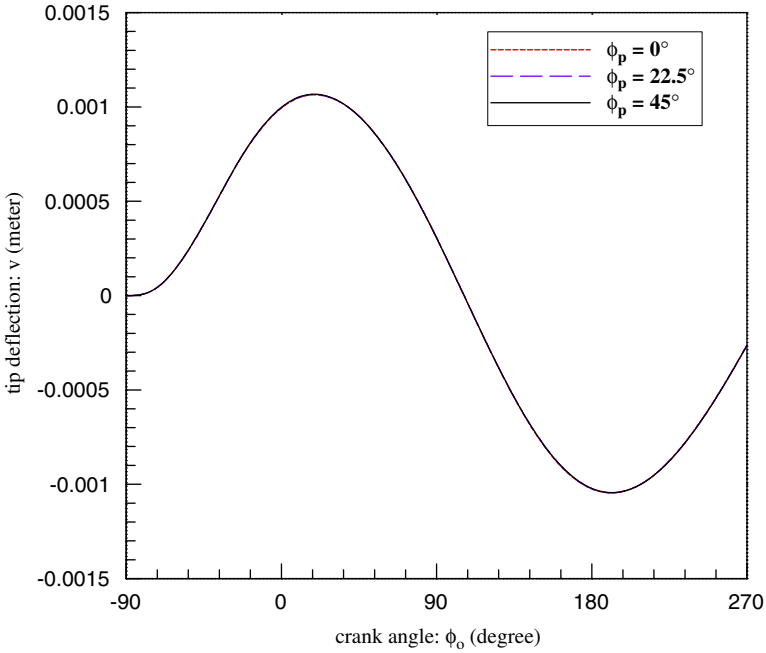

Fig. 14. The tip deflection v for coupled system with different gear pressure angle: $\phi_p = 0°$, 22.5°, 45°.

The influence of the shaft radius on the coupled system is also studied. Fig. 16 shows that the smaller shaft radius induces a little larger tip deflection. This may be explained that thinner shaft is more flexible and causes larger coupling effect on the mechanism. However, a gear shaft is seldom designed to be a thin one to drive a quick-return mechanism in a practical device. It is seen that the tip deflections are very close when the shaft radii is of 18.5 and 27.5 mm. This means when the shaft radius exceeds some value, the flexibility is dominated by the other components of the geared rotor.

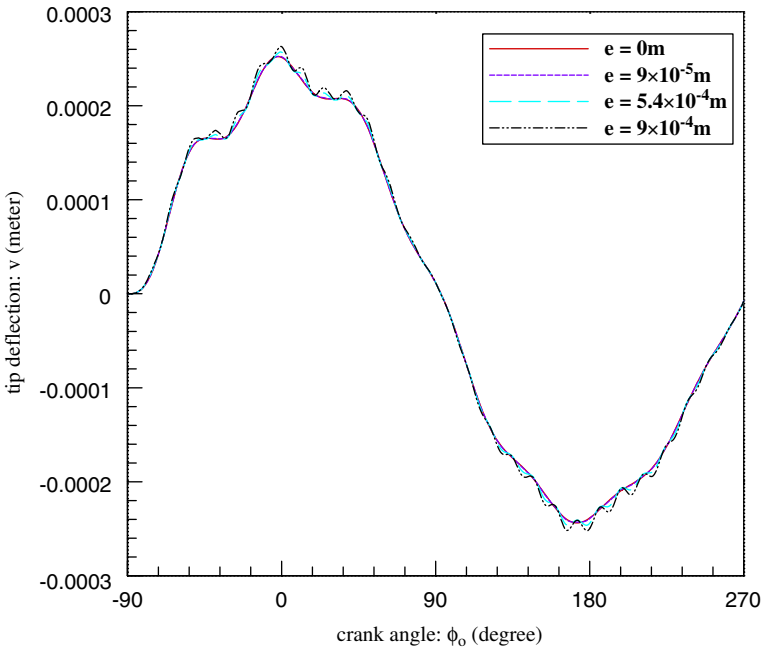

Fig. 15. The tip deflection v for coupled system with $k_b = 10^7$ N/m and different amplitude of transmission error: $e = 0$, 9×10^{-5}, 5.4×10^{-4}, 9×10^{-4} m.

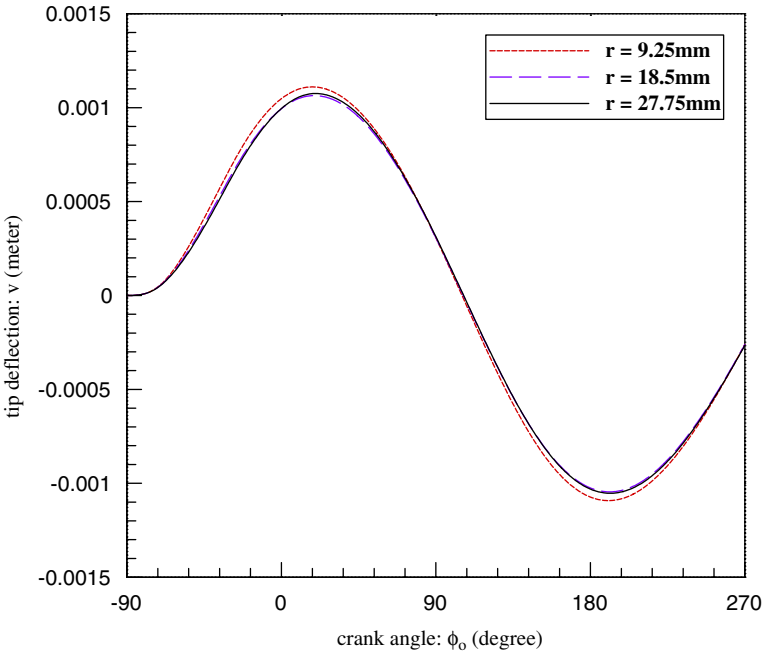

Fig. 16. The tip deflection v for coupled system with different radius of shaft: $r = 9.25$, 18.5, 27.75 mm.

4. Conclusion

Based on the characteristic that the geared rotor dynamics can influence the motion of the quick-return mechanism to some extent, the coupled system of the geared rotor and the quick-return mechanism is

suggested to be concerned for improving the accuracy and efficiency of the mechanism. In this study, the finite element model of the coupled system is formulated and the system equation of motion is derived based on Hamilton's principle. A longer crank induces larger tip deflection for both the coupled and uncoupled systems. The parameters including the bearing properties, and the shaft radius are taken into account to study the coupling effect of the geared rotor on the quick-return mechanism. It is indicated that for the studied case the small values of bearing stiffness and shaft radius induce large vibration amplitudes of the rod tip. The bearing damping can suppress the oscillation of the tip deflection. The transmission error of gear mesh induces high frequency oscillation. The coupled model will increase the accuracy of dynamic response of mechanism and the parameter study leads to the future works such as system optimization and system automatic control.

Acknowledgments

The author is very thankful to the National Science Council of Taiwan for the Grant NSC 92-2212-E-344-008 to carry out this project.

References

[1] J.S. Rao, *Rotor Dynamics*, second ed., Wiley, New York, 1992.
[2] M. Lalanne, G. Ferrairs, *Rotor Dynamics Prediction in Engineering*, Wiley, New York, 1991.
[3] K.H. Saling, Th. Schwinder, Variations in design and principles of dimensioning of rotors for hydroelectric generators, bending critical speeds, structural resources and torsional vibration stresses; evaluation criteria for the vibration of bearing and rotor unbalance, Report 138, CIGRE, 1966.
[4] J. Lund, Critical speed, stability and response of a geared train of rotors, *Journal of Mechanical Design, Transactions of the ASME* 100 (1978) 535.
[5] A. Kahraman, H. Nevzat Ozguven, D.R. Houser, J.J. Zakrajsek, Dynamics analysis of geared rotors by finite elements, *Journal of Mechanical Design, Transactions of the ASME* 114 (1992) 507.
[6] T.N. Shiau, Y.W. Chou, J.R. Chang, H.D. Nelson, A study on the dynamic characteristics of geared rotor-bearing system with hybrid method, *International Gas Turbine and Aeroengine Congress and Exposition*, The Hague, Netherlands, 1994.
[7] J.S. Rao, J.R. Chang, T.N. Shiau, Coupled bending-torsional vibration of geared rotors. *ASME Design Engineering Technical Conference*, *DE-Vol. 84-2*, vol. 3, Part B, 1995, p. 977.
[8] S.T. Choi, S.Y. Mau, Dynamic analysis of geared rotor-bearing systems by the transfer matrix method, *Journal of Mechanical Design, Transactions of the ASME* 123 (2001) 563.
[9] E.J. Gunter, Influence of flexibility mounted rolling element bearings on rotor response, part 1: linear analysis, *Journal of Lubrication Technology* 92 (1) (1970) 59.
[10] D.W. Childs, K. Graviss, A note on critical-speed solutions for finite-element-based rotor models, *Journal of Mechanical Design* 104 (1) (1982) 412.
[11] D.G. Beale, R.A. Scott, The stability and response of a flexible rod in a quick-return mechanism, *Journal of Sound and Vibration* 141 (2) (1990) 277.
[12] D.G. Beale, R.A. Scott, The stability and response of a flexible rod in a quick-return mechanism: large crank case, *Journal of Sound and Vibration* 166 (3) (1993) 463.
[13] M.O. Okuyiga, W.H. Ray, Modelling and estimation for a moving boundary problem, *International Journal for Numerical Methods in Engineering* 21 (1985) 601.
[14] H.P. Lee, Dynamics of a flexible rod in a quick-return mechanism, *Journal of Mechanical Design, Transactions of the ASME* 116 (1994) 70.
[15] J.O. Song, E.J. Haug, Dynamic analysis of planar flexible mechanisms, *Computer Methods in Applied Mechanics and Engineering* 24 (1980) 359.
[16] Z. Yang, J.P. Sadler, Large-displacement finite element analysis of flexible linkages, *Journal of Mechanical Design, Transactions of the ASME* 112 (1990) 175.
[17] R.F. Fung, F.Y. Lee, Dynamic analysis of the flexible rod of a quick-return mechanism with time-dependent coefficients by the finite element method, *Journal of Sound and Vibration* 202 (2) (1997) 187.
[18] A. Shabana, B. Thomas, Chatter vibration of flexible multibody machine tool mechanisms, *Mechanism and Machine Theory* 22 (4) (1987) 359.
[19] R.F. Fung, K.W. Chen, Vibration suppression and motion control of a non-linearly coupled flexible quick-return mechanism driven by a PM synchronous servo motor, *Journal of Sound and Vibration* 212 (4) (1998) 721.
[20] M. Stylianou, B. Tabarrok, Finite element analysis of an axially moving beam, part I: time integration, *Journal of Sound and Vibration* 178 (1994) 433.
[21] B.O. Al-Bedoor, Y.A. Khulief, Finite element dynamic modeling of a translating and rotating flexible link, *Computer Methods in Applied Mechanics and Engineering* 131 (1996) 173.
[22] B.O. Al-Bedoor, Y.A. Khulief, General planar dynamics of a sliding flexible link, *Journal of Sound and Vibration* 206 (1997) 641.
[23] E.N. Parviz, *Computer-Aided Analysis of Mechanical System*, Prentice-Hall International Edition, Englewood Cliffs, NJ, 1988 pp. 42–46.